

# The rotation of Mimas

B. Noyelles<sup>\*1,2</sup>, Ö. Karatekin<sup>3</sup>, and N. Rambaux<sup>4,2</sup>

- <sup>1</sup> FUNDP-University of Namur - Department of Mathematics & NAMur Center for Complex SYStems (NAXYS) - Rempart de la Vierge 8 - B-5000 Namur - Belgium  
<sup>2</sup> IMCCE, Paris Observatory, UPMC, Univ. Lille 1, CNRS UMR 8028 - 77 avenue Denfert Rochereau - F-75014 Paris - France  
<sup>3</sup> Royal Observatory of Belgium - Ringlaan 3 - B-1180 Brussels - Belgium  
<sup>4</sup> Université Pierre et Marie Curie Paris 6 - 4 place Jussieu - F-75005 Paris - France

Received / Accepted

## ABSTRACT

**Context.** The Cassini mission in the Saturnian system is an outstanding opportunity to improve our knowledge of the satellites of Saturn. The data obtained thanks to this mission must be confronted to theoretical models.

**Aims.** This paper aims at modeling the rotation of Mimas, with respect to its possible internal structure.

**Methods.** For that, we first build different interior models, in considering Mimas as composed of 2 rigid layers with different porosity. Then we simulate the rotational behavior of these models in a 3-degree of freedom numerical code, in considering complete ephemerides of a Mimas whose rotation is disturbed by Saturn. We also estimate the deviation of its longitudinal orientation due to tides.

**Results.** We expect a signature of the internal structure up to  $0.53^\circ$  in the longitudinal librations and an obliquity between 2 and 3 arcmin, the exact values depending on the interior.

**Conclusions.** The longitudinal librations should be detectable, inverting them to get clues on the internal structure of Mimas is challenging.

**Key words.** Planets and satellites: individual: Mimas – Planets and satellites: interiors – Celestial mechanics

## 1. Introduction

The Cassini spacecraft gives us the unique opportunity to have accurate set of geodetic data for icy satellites of Saturn as for example, the shape, the gravitational field, the rotational data (Thomas, 2010). The flybys of Mimas have provided high resolution images of the surface in the finest detail yet seen (Roatsch et al., 2009). Cassini spacecraft has detected temperature inhomogeneities (Howett et al., 2011), usually attributed to exogenic process. The theoretical model of Mimas rotational state can be used to interpret the Cassini data and to better understand its interior and evolution.

Like for our Moon, Mimas is in synchronous rotation and shows almost the same face towards Saturn. Moreover, it is considered to have a large librational amplitude (Comstock & Bills, 2003). The rotational state of a synchronous body depends on the distribution of mass of the body, and therefore it is a signature of its internal structure. Here, we propose to model the rotation of Mimas considering it as a rigid body. A highly rigid interior of Mimas for most of its history is consistent with its un-relaxed shape (Thomas et al., 2007; Thomas, 2010).

Since the distant spacecraft flybys of Mimas do not allow the determination of the GM nor the gravity harmonics, the mass of Mimas is determined from an analysis of its orbital resonances with Tethys and Methone (Jacobson et al., 2006). Moreover, its internal structure remains uncertain. The mean density of  $1.15 \text{ g cm}^{-3}$  suggests that Mimas is made of homogenous mixture of ice and rocks. The observed shape of

Mimas by Voyager has been interpreted as an indication of interior mass concentration which can be either due to internal differentiation (Dermott & Thomas, 1988) or radially variable porosity (Eluszkiewicz, 1990). However, Cassini observations showed that Mimas' shape, although a triaxial ellipsoid, is departed slightly from hydrostatic shape and therefore interpreting the interior configuration from the shape is limited (Thomas et al., 2007; Thomas, 2010). In the present study, we consider Mimas to be composed of two rigid layers. We consider both hydrostatic and non-hydrostatic interior models. The interior models considering compaction of ice-silica particle mixtures (Yasui & Arakawa, 2009) are expected to yield realistic principal moment of inertia  $A < B < C$  (Eluszkiewicz, 1990). Since Mimas orbits close to its parent planet, the present-day diurnal tidal stresses can be important, and we took the tidal effects into account as well.

The paper is structured as follows: we first model the internal structure of Mimas, in considering two different assumptions: that Mimas is in hydrostatic equilibrium, and that its ellipsoid of gravity is proportional to its ellipsoid of shape. From these two assumptions we derive 23 models of Mimas. Then we perform numerical integrations of the rotation of these "Mimasses" in a full 3-degree of freedom conservative models. Finally, we check the influence of the tides on the equilibrium orientation of Mimas' long axis.

## 2. Internal structure

Interior structure models of planets and natural satellites are in general non-unique due to the presence of fewer constraints than unknowns. For Mimas we have only two constraints: the mean radius  $R$  and the mean density  $\rho$ , or the Mass  $m$  (Tab.1). In this

Send *offprint requests* to: B. Noyelles, e-mail: benoit.noyelles@fundp.ac.be

\* F.R.S.-FNRS post-doctoral research fellow

**Table 1.** Physical and dynamical properties of Mimas, used in the calculations. The mean density  $\rho$  has been calculated from the radius of Thomas et al. (2007) and the mass of Jacobson et al. (2006). A recent paper by Thomas (2010) slightly shifts the mean radius to 198.3, the change has negligible effects. However, we use this last reference for the triaxial shape of Mimas, because the rotation, especially the longitudinal motion, is sensitive to the differences between these axes.

Parameter	Value	Source
Mean motion $n$	2435.14429644 rad/y	TASS1.6 (Vienne & Duriez, 1995)
Mean radius $R$	198.2 km	(Thomas et al., 2007)
Density $\rho$	1150.03 $kg.m^{-3}$	(Thomas et al., 2007)
Mass $m$	$3.7495 \times 10^{19}$ kg	(Jacobson et al., 2006)
Saturn-facing radius $a$	207.8 km	(Thomas, 2010)
Orbit facing radius $b$	196.7 km	(Thomas, 2010)
Polar radius $c$	190.6 km	(Thomas, 2010)

study where we deal with the rotation, the moment of inertia differences are the main point of interest.

Because we have only few constraints, we prefer to have as simple interior structure models as possible. We assume a two-layer interior structure model with a rocky core and icy mantle. The models with variable porosity supported by recent compaction experiments (Yasui & Arakawa, 2009), yield realistic moments of inertia (Eluszkiewicz, 1990). The mean density of Mimas is close to the density of water ice and the interior is consistent with an icy mantle and small rocky core, alternatively Mimas can be homogenous with a variable or constant porosity.

With Mimas' figure departed from hydrostatic shape (Thomas et al., 2007; Thomas, 2010) and without the knowledge of  $C_{22}$  and  $J_2$ , we do not know the moment of inertia differences. As it is the case for the Moon (see e.g. Lambeck & Pullan (1980)), the internal mass distribution could be a fossil shape which dates back from an earlier orbital position where the tidal heating was important with higher orbital eccentricity and obliquity or a frozen shape following a large impact. Mimas shows a heavily cratered surface without signs of geological activity for billions of years. Its large free eccentricity gives another reason for low internal activity. This anomalously large eccentricity of Mimas can be explained by passage through several past resonances (Meyer & Wisdom, 2008). Determination of the gravity coefficients  $C_{22}$  and  $J_2 = -C_{20}$  are necessary to conclude on the hydrostatic equilibrium because the figure of Mimas may not represent the real flattening or the internal mass determination as it is the case for Titan (Zebker, 2009). As suggested by Johnson et al. (2006), large impact craters and heating of Mimas' hemispheres by Saturn at different amounts may be potential sources of large non-hydrostatic anomalies that could impede accurate interpretation of the shape data

### 2.1. Hydrostatic approximation

Since we do not know the gravity coefficients  $C_{22}$  and  $J_2$ , we will use a simple approach. For a two layer interior model the core radius  $R_c$  can be determined if the densities of the rocky core  $\rho_c$  and the icy mantle  $\rho_s$  are known, i.e.

$$R_c = R \left( \frac{\rho - \rho_s}{\rho_c - \rho_s} \right)^{1/3}. \quad (1)$$

The moment of Inertia factor ( $MOI = I_p/(MR^2)$ ) is given as:

$$MOI = \frac{2}{5} \left( \frac{(\rho - \rho_s)^{5/3}}{\rho(\rho_c - \rho_s)^{2/3}} + \frac{\rho_s}{\rho} \right). \quad (2)$$

The Fig. 1 shows that in the absence of additional constraints, plausible density values of the core and icy shell yield  $0.3 <$

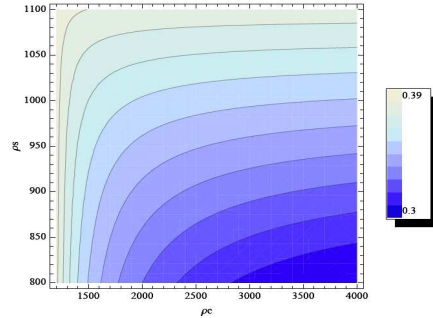


**Fig. 1.** Variations of the Moment of Inertia factor (MOI) with icy shell and rocky core densities.

$MOI < 0.4$ . The range of MOI is used to estimate the moment of inertia of tri-axial Mimas, as shown below.

For a satellite in hydrostatic equilibrium,  $MOI$  is related to the fluid Love number  $k_f$  which describes the relation of the satellite to a perturbing potential after all viscous stresses have relaxed (Munk & MacDonald, 1960; Hubbard & Anderson, 1978):

$$MOI = \frac{2}{3} \left[ 1 - \frac{2}{5} \sqrt{\frac{4 - k_f}{1 + k_f}} \right], \quad (3)$$

and the gravity coefficients  $C_{22}$  and  $J_2$  are determined from (Rappaport et al., 1997):

$$C_{22} = \frac{k_f}{4} q_r + O(q_r^2), \quad (4)$$

$$J_2 = \frac{5k_f}{6} q_r + O(q_r^2), \quad (5)$$

where  $q_r = \Omega^2 R^3 / (Gm)$ ,  $\Omega$  being the spin velocity of Mimas, equal to its mean motion  $n$  since Mimas is in synchronous rotation. With the numerical values given in Tab.1, we have  $q_r = 0.01854$ .

The differences between the three principal moments of inertia  $A < B < C$  are determined from the definitions of  $C_{22}$  and  $J_2$ , i.e.:

$$B - A = 4C_{22}MR^2,$$

$$C - A = (J_2 + 2C_{22})MR^2,$$

$$C - B = (J_2 - 2C_{22})MR^2.$$

The relationship between the mean moment of inertia  $I = \frac{A+B+C}{3}$  and the polar moment of inertia  $C$  is:

$$C = I + \frac{2}{3}J_2MR^2. \quad (6)$$

We can then calculate all the three moments of inertia  $A$ ,  $B$  and  $C$ .

## 2.2. Nonhydrostatic shape

We here use the observed shape ( $a = 207.8$  km,  $b = 196.7$  km,  $c = 190.6$  km, Thomas (2010)) to calculate the moments of inertia of Mimas, in assuming that the shape of the core is proportional to the one of Mimas, i.e. we assume

$$\frac{a_c}{a} = \frac{b_c}{b} = \frac{c_c}{c} = \frac{R_c}{R}, \quad (7)$$

where  $a_c$ ,  $b_c$  and  $c_c$  are the dimensions of the core, and  $R_c$  its mean radius (Eq.1).

A quadrature over the volume of respectively the core and the shell gives

$$\begin{aligned} C_c &= \iiint_{core} \rho_c (x^2 + y^2) dx dy dz \\ &= \frac{4}{15} \pi a_c b_c c_c (a_c^2 + b_c^2) \rho_c \\ &= \frac{4}{15} \pi abc (a^2 + b^2) \rho_c \left(\frac{R_c}{R}\right)^5, \end{aligned} \quad (8)$$

$$\begin{aligned} C_s &= \iiint_{Mimas} \rho_s (x^2 + y^2) dx dy dz \\ &\quad - \iiint_{core} \rho_s (x^2 + y^2) dx dy dz \\ &= \frac{4}{15} \pi abc (a^2 + b^2) \rho_c \left[1 - \left(\frac{R_c}{R}\right)^5\right]. \end{aligned} \quad (9)$$

We then get  $C = C_c + C_s$ . The other moments of inertia  $A$  and  $B$  being obtained similarly, we have

$$A = \frac{4}{15} \pi abc (b^2 + c^2) \left[ (\rho_c - \rho_s) \left(\frac{R_c}{R}\right)^5 + \rho_s \right], \quad (10)$$

$$B = \frac{4}{15} \pi abc (a^2 + c^2) \left[ (\rho_c - \rho_s) \left(\frac{R_c}{R}\right)^5 + \rho_s \right], \quad (11)$$

$$C = \frac{4}{15} \pi abc (a^2 + b^2) \left[ (\rho_c - \rho_s) \left(\frac{R_c}{R}\right)^5 + \rho_s \right]. \quad (12)$$

We finally see that the ratio of the moments of inertia  $A/C = (b^2 + c^2)/(a^2 + b^2)$  and  $B/C = (a^2 + c^2)/(a^2 + b^2)$  are independent on the mean radius  $R_c$  and density  $\rho_c$  of the core, so every model of the internal structure of Mimas based on its observed shape (in neglecting the uncertainties on the radii  $a$ ,  $b$  and  $c$ ) will present the same rotational response.

The interior models considered in the present study are gathered in Tab.2.

## 3. Computing the rotation of Mimas

In this Section, Mimas is assumed to be a two-layers rigid body and the tidal contributions will be investigated in the Section 5.

Its rotation is highly constrained by the gravitational perturbation of Saturn, and so depends on the variations of the distance Mimas-Saturn. That is the reason why we must understand the orbital dynamics of Mimas before investigating its rotation.

### 3.1. The orbital dynamics of Mimas

Mimas is the smallest of the main Saturnian satellites, and also the closest to its parent planet and the rings. Discovered by Herschel in 1789, it is known since Struve (1891) to be in 2:1 mean-motion resonance with Tethys. More precisely, these two bodies are locked in an inclination-type resonance whose argument is  $2\lambda_1 - 4\lambda_3 + \varrho_{\lambda_1} + \varrho_{\lambda_3}$ , the subscript 1 standing for the satellite S-1 Mimas, 3 for S-3 Tethys,  $\lambda_i$  being the mean longitudes, and  $\varrho_{\lambda_i}$  the longitudes of the ascending nodes. This resonance tends to raise the inclinations of the satellites to  $\approx 1.5^\circ$  for Mimas and  $\approx 1^\circ$  for Tethys (Allan, 1969), and stimulates librations of the resonant argument around 0 with an amplitude of  $\approx 95^\circ$  and a period of  $\approx 70$  years. The trapping of the system into this resonance can be explained in considering a non-null eccentricity for Tethys that induces secondary resonances that strongly enhances the capture probability (Champanois & Vienne, 1999a,b).

It is convenient to work on a Fourier-type representation of the orbital motion of Mimas that allows to identify every proper mode of the motion. The basic idea is that the variables describing the orbital motion of Mimas can be represented as quasi-periodic series (and a slope for precessing angles like the ascending node, the pericenter and the mean longitude), i.e. infinite but converging sums of trigonometric series. The arguments of these series can be expressed as integer combination of a few proper modes of constant frequencies. The existence of these modes comes both from the KAM (Arnold, 1963; Moser, 1962) and the Nekhoroshev theories (Nekhoroshev, 1977, 1979). The KAM theory states that for a quasi-integrable Hamiltonian system (i.e. like  $\mathcal{H} = \mathcal{H}_0 + \epsilon\mathcal{H}_1$  where  $\mathcal{H}_0$  is an integrable Hamiltonian and  $\epsilon\mathcal{H}_1$  a small perturbation) verifying classical assumptions, the motion can be considered to be on invariant tori (i.e. with constant amplitudes and angles depending linearly on time) in action-angle coordinates. For a bigger perturbation the Nekhoroshev theory says that the invariant tori survive over a timescale that is exponentially long with respect to the invert of the amplitude of the perturbation  $\epsilon$ , provided that the Hamiltonian of the system presents a property of steepness, that is an extension of the convexity.

Such a representation is given by TASS1.6 ephemerides (Vienne & Duriez, 1995) where the orbital motion of Mimas can be described using the 5 proper modes  $\lambda$ ,  $\omega$ ,  $\phi$ ,  $\zeta$  and  $\Phi$ .  $\lambda$  is the linear part of Mimas' mean longitude,  $\omega$  is the main oscillation mode of the librations of the resonant argument  $2\lambda_1 - 4\lambda_3 + \varrho_{\lambda_1} + \varrho_{\lambda_3}$ ,  $\zeta$  (called  $\rho_1$  in (Vienne & Duriez, 1995)) is the mean slope of  $\lambda_1 - 2\lambda_3$ , and  $\phi - \zeta$  and  $\Phi - \zeta$  are the mean slopes of respectively the longitudes of the pericenter of Mimas and its ascending node. The values of the frequency associated are gathered in Tab.3.

### 3.2. Rotational model

As for most of the natural satellites of the Solar System, Mimas is expected to follow the 3 Cassini Laws, originally described for the Moon (Cassini, 1693; Colombo, 1966), i.e.:

**Table 2.** The interior models considered in the present study. The first 22 cases have been elaborated in considering Mimas as in hydrostatic equilibrium, while the 23<sup>rd</sup> is based on the observed shape. We give only one possibility for the shape model because the ratios of the moments of inertia  $A/C$  and  $B/C$  remain constant, so the rotational response of Mimas is the same for any interior model based on the shape.

N	$\rho_c$	$\rho_s$	$k_f$	MOI	$J_2 (10^{-2})$	$C_{22} (10^{-3})$	$C/(mR^2)$
1	1200	800	1.40473	0.389636	2.17051	6.51152	0.404106
2	1500	800	1.11293	0.354953	1.71963	5.15889	0.366418
3	2000	800	0.94032	0.331801	1.45293	4.35878	0.341487
4	2500	800	0.86349	0.320705	1.33422	4.00267	0.329600
5	3000	800	0.81885	0.314001	1.26524	3.79571	0.322436
6	3500	800	0.78921	0.309439	1.21944	3.65831	0.317569
7	4000	800	0.76788	0.306100	1.18649	3.55946	0.314010
8	1200	1000	1.41613	0.390899	2.18812	6.56437	0.405486
9	1500	1000	1.24455	0.371206	1.92301	5.76902	0.384026
10	2000	1000	1.17336	0.362551	1.81300	5.43901	0.374638
11	2500	1000	1.14536	0.359061	1.76975	5.30925	0.370860
12	3000	1000	1.12980	0.357099	1.74570	5.23711	0.368737
13	3500	1000	1.11969	0.355816	1.73009	5.19026	0.367350
14	4000	1000	1.11251	0.354901	1.71899	5.15698	0.366361
15	1200	1100	1.44040	0.393565	2.22563	6.67688	0.408403
16	1500	1100	1.38066	0.386951	2.13331	6.39993	0.401173
17	2000	1100	1.36451	0.385134	2.10836	6.32508	0.399189
18	2500	1100	1.35879	0.384487	2.09953	6.29858	0.398484
19	3000	1100	1.35572	0.384139	2.09478	6.28435	0.398105
20	3500	1100	1.35376	0.383917	2.09176	6.27527	0.397862
21	4000	1100	1.35239	0.383761	2.08963	6.26890	0.397692
22	1150.03	1150.03	1.5	0.400000	2.30951	6.92854	0.415397
23	1200	800	1.40473	0.389636	2.28639	5.57013	0.406273

**Table 3.** The proper frequencies of Mimas' orbital motion (from TASS1.6 (Vienne & Duriez, 1995)).

	Frequency (rad/y)	Period (d)	Period (y)
$\lambda$	2435.14429644	0.942421949	$2.580211 \times 10^{-3}$
$\omega$	0.08904538	25772.62777	70.561609
$\phi$	10.19765304	225.0452555	0.616140
$\zeta$	3.81643833	601.3285779	1.646348
$\Phi$	-2.55544336	898.0568575	2.458746

1. The Moon rotates uniformly about its polar axis with a rotational period equal to the mean sidereal period of its orbit about the Earth.
2. The inclination of the Moon's equator to the ecliptic is a constant angle (approximately  $1.5^\circ$ ).
3. The ascending node of the lunar orbit on the ecliptic coincides with the descending node of the lunar equator on the ecliptic. This law could also be expressed as: the spin axis and the normals to the ecliptic and orbit plane remain coplanar.

In the case of natural satellites, they can be rephrased this way: the rotation of the satellite is synchronous, its angular momentum has a nearly constant inclination on an inertial reference plane, and is located in the plane defined by the normal to the orbital plane and to the Laplace Plane. The Laplace Plane is the plane normal to the rotation axis of the orbital frame, i.e. it is defined with respect to the orbital precessional motion. It has the property to minimize the variations of the orbital inclinations. For satellites orbiting close to their planet as it is the case here, the equatorial plane of Saturn is so close to the Laplace Plane that it can be used for describing the rotational dynamics.

Our rotational model is similar to the one already used in e.g. (Noyelles et al., 2008; Noyelles, 2010) for studying the rigid rotation of the Saturnian satellites Titan, Janus and Epimetheus.

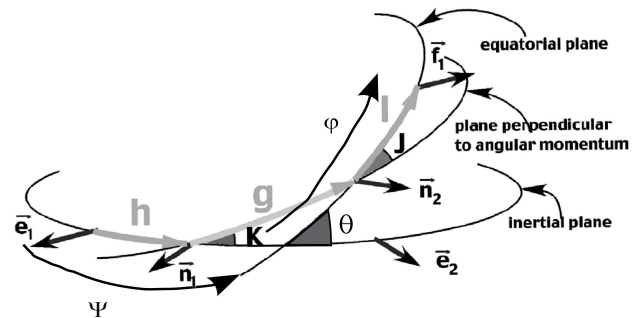


**Fig. 2.** The Andoyer variables (partially reproduced from (Henrard, 2005a)).

We consider Mimas as a rigid triaxial body whose matrices of inertia reads

$$I = \begin{pmatrix} A & 0 & 0 \\ 0 & B & 0 \\ 0 & 0 & C \end{pmatrix} \quad (13)$$

with  $A \leq B \leq C$ .

The dynamical model is a 3-degree of freedom one. We will use the Andoyer variables which requires a decomposition with 3 references frames :

1. An inertial reference frame  $(e_1, e_2, e_3)$ . We used the one in which the orbital ephemerides are given, i.e. mean Saturnian equator and mean equinox for J2000.0 epoch.
2. A frame  $(n_1, n_2, n_3)$  bound to the angular momentum of Mimas.
3. A frame  $(f_1, f_2, f_3)$  rigidly linked to Mimas.

We first use Andoyer's variables (Andoyer, 1926; Deprit, 1967), which are based on two linked sets of Euler's angles. The

first set  $(h, K, g)$  locates the position of the angular momentum in the first frame  $(e_1, e_2, e_3)$ , while the second one,  $(g, J, l)$ , locates the body frame  $(f_1, f_2, f_3)$  in the second frame tied to the angular momentum (see Fig. 2).

The canonical set of Andoyer's variables consists of the three angular variables  $l, g, h$  and their conjugated momenta  $L, G, H$  defined by the norm  $G$  of the angular momentum and two of its projections:

$$\begin{aligned} l, & & L = G \cos J, \\ g, & & G, \\ h, & & H = G \cos K. \end{aligned} \quad (14)$$

Unfortunately, these variables present two singularities: when  $J = 0$  (i.e., the angular momentum is colinear to  $f_3$ ),  $l$  and  $g$  are undefined, and when  $K = 0$  (i.e., when Mimas' principal axis of inertia is perpendicular to its orbital plane),  $h$  and  $g$  are undefined. That is the reason why we shall use the modified Andoyer's variables:

$$\begin{aligned} p = l + g + h, & & P = \frac{G}{nC}, \\ r = -h, & & \mathcal{R} = \frac{G-H}{nC} = P(1 - \cos K), \\ & & = 2P \sin^2 \frac{K}{2}, \\ \xi_q = \sqrt{\frac{2Q}{nC}} \sin q, & & \eta_q = \sqrt{\frac{2Q}{nC}} \cos q, \end{aligned} \quad (15)$$

where  $n$  is the body's mean orbital motion,  $q = -l$ , and  $Q = G - L = G(1 - \cos J) = 2G \sin^2 \frac{J}{2}$ . With these new variables, the singularity on  $l$  has been dropped. Using these variables has a great mathematical interest, because they are canonical, so they simplify an analytical study of the system, as was done in the previous works mentioned above. Our study here is essentially numerical, but we keep these variables, in order to be consistent with previous studies. We later derive other output variables, that are more relevant from a physical point of view.

In these variables, the kinetic energy  $T = \frac{1}{2}\omega \cdot \mathbf{G}$  of the system reads:

$$\begin{aligned} T = & \frac{nP^2}{2} + \frac{n}{8}[4P - \xi_q^2 - \eta_q^2] \\ & \times \left[ \frac{\gamma_1 + \gamma_2}{1 - \gamma_1 - \gamma_2} \xi_q^2 + \frac{\gamma_1 - \gamma_2}{1 - \gamma_1 + \gamma_2} \eta_q^2 \right] \end{aligned} \quad (16)$$

with

$$\gamma_1 = \frac{2C - A - B}{2C} = J_2 \frac{MR^2}{C} \quad (17)$$

and

$$\gamma_2 = \frac{B - A}{2C} = 2C_{22} \frac{MR^2}{C}. \quad (18)$$

In these last 3 formulae,  $\omega$  is the instantaneous vector of rotation,  $M$  is the mass of Mimas,  $R$  its mean radius, and  $J_2$  and  $C_{22}$  the two classical normalized gravitational coefficients related respectively to the oblateness and equatorial ellipticity of the considered body.

The gravitational disturbing potential due to an oblate perturber  $p$  reads (Henrard, 2005c):

$$V_p = V_{p1} + V_{p2} \quad (19)$$

with

$$V_{p1} = -\frac{3}{2}C \frac{\mathcal{G}M_p}{d_p^3} [\gamma_1(x_p^2 + y_p^2) + \gamma_2(x_p^2 - y_p^2)] \quad (20)$$

and

$$\begin{aligned} V_{p2} = & -\frac{15}{4}CJ_{2p} \frac{\mathcal{G}M_p}{d_p^3} \left(\frac{R_p}{d_p}\right)^2 \\ & \times [\gamma_1(x_p^2 + y_p^2) + \gamma_2(x_p^2 - y_p^2)], \end{aligned} \quad (21)$$

where  $\mathcal{G}$  is the gravitational constant,  $M_p$  the mass of the perturber,  $J_{2p}$  its  $J_2$ ,  $R_p$  its mean radius,  $d_p$  the distance between the perturber's and Mimas' centers of mass, and  $x_p$  and  $y_p$  the two first components of the unit vector pointing to the center of mass of the perturber, from the center of mass of the body, in the reference frame  $(f_1, f_2, f_3)$ .  $V_{p1}$  expresses the perturbation due to a pointmass perturber, while  $V_{p2}$  represents the perturbation due to its  $J_2$ , assuming that the body is in the equatorial plane of the perturber. As shown in (Henrard, 2005c), it is a good approximation if the sine of the angle between Saturn's equatorial plane and the orbit is small. In the case of Mimas, this angle (i.e. Mimas' orbital inclination) is  $\approx 1.5^\circ \approx 2.6 \times 10^{-2}$  rad, so we can consider that its sine is always smaller than  $3 \times 10^{-2}$ . This assertion also assumes that the obliquity of Mimas is very small, what will be checked in this study.

Usually the orbital ephemerides give us the location of the perturber in the inertial frame, so we have to perform 5 rotations to convert the coordinates from the inertial frame to  $(f_1, f_2, f_3)$ . More precisely, if we name  $(x_i, y_i, z_i)^T$  the unit vector locating the perturber's center of mass in the inertial frame, we have

$$\begin{pmatrix} x_p \\ y_p \\ z_p \end{pmatrix} = R_3(-l)R_1(-J)R_3(-g)R_1(-K)R_3(-h) \begin{pmatrix} x_i \\ y_i \\ z_i \end{pmatrix} \quad (22)$$

with

$$R_3(\phi) = \begin{pmatrix} \cos \phi & -\sin \phi & 0 \\ \sin \phi & \cos \phi & 0 \\ 0 & 0 & 1 \end{pmatrix} \quad (23)$$

and

$$R_1(\phi) = \begin{pmatrix} 1 & 0 & 0 \\ 0 & \cos \phi & -\sin \phi \\ 0 & \sin \phi & \cos \phi \end{pmatrix}. \quad (24)$$

Finally, the total Hamiltonian of the problem reads:

$$\begin{aligned} H = & \frac{nP^2}{2} + \frac{n}{8}[4P - \xi_q^2 - \eta_q^2] \\ & \times \left[ \frac{\gamma_1 + \gamma_2}{1 - \gamma_1 - \gamma_2} \xi_q^2 + \frac{\gamma_1 - \gamma_2}{1 - \gamma_1 + \gamma_2} \eta_q^2 \right] \\ & - \frac{3}{2n} \frac{\mathcal{G}M_{\mathfrak{h}}}{d_{\mathfrak{h}}^3} \left(1 + \frac{5}{2}J_{2\mathfrak{h}} \left(\frac{R_{\mathfrak{h}}}{d_{\mathfrak{h}}}\right)^2\right) \\ & \times [\gamma_1(x_{\mathfrak{h}}^2 + y_{\mathfrak{h}}^2) + \gamma_2(x_{\mathfrak{h}}^2 - y_{\mathfrak{h}}^2)], \end{aligned} \quad (25)$$

where the index  $\mathfrak{h}$  stands for Saturn. We will use this Hamiltonian for a numerical study of the rotation. An analytical study can show that the Hamiltonian (25) can be reduced to

$$\mathcal{H}(u, v, w, U, V, W) = \omega_u U + \omega_v V + \omega_w W + \mathcal{P}(u, v, w, U, V, W) \quad (26)$$

where  $\mathcal{P}$  represents a perturbation, and the three constants  $\omega_u$ ,  $\omega_v$  and  $\omega_w$  are the periods of the free oscillations around the equilibrium defined by the Cassini Laws. This last Hamiltonian is obtained after several canonical transformations, the first one consisting in expressing the resonant arguments  $\sigma = p - \lambda + \pi$  and  $\rho = r + \Omega$  respectively associated with the 1:1 spin-orbit resonance and with the orientation of the angular momentum,  $\lambda$  and  $\Omega$  being the orbital variables defined above. The complete calculation is beyond the scope of this paper, the reader can find details in (Henrard, 2005a,b; Noyelles et al., 2008).

### 3.3. A numerical study

In order to integrate numerically the system, we first express the coordinates of the perturber  $(x_{\tilde{\gamma}}, y_{\tilde{\gamma}})$  with the numerical ephemerides and the rotations given in (Eq.22), in the body frame  $(f_1, f_2, f_3)$ . As explained before, the ephemerides are given by the TASS1.6 ephemerides (Vienne & Duriez, 1995). This way, we get coordinates depending of the canonical variables. Then we derive the equations coming from the Hamiltonian (25):

$$\begin{aligned} \frac{dp}{dt} &= \frac{\partial H}{\partial P}, & \frac{dP}{dt} &= -\frac{\partial H}{\partial p}, \\ \frac{dr}{dt} &= \frac{\partial H}{\partial R}, & \frac{dR}{dt} &= -\frac{\partial H}{\partial r}, \\ \frac{d\xi_q}{dt} &= \frac{\partial H}{\partial \eta_q}, & \frac{d\eta_q}{dt} &= -\frac{\partial H}{\partial \xi_q}. \end{aligned} \quad (27)$$

We integrated over 200 years using the Adams-Bashforth-Moulton 10th order predictor-corrector integrator. The solutions consist of two parts, the forced one, directly due to the perturbation, and the free one, that depends on the initial conditions. The initial conditions should be as close as possible to the exact equilibrium, that is assumed to be the Cassini State 1 in 1:1 spin-orbit resonance, to have low amplitudes of the free librations. For that, we have used the iterative algorithm NAFFO (Noyelles et al., 2011) to remove the free librations from the initial conditions, after they have been identified by frequency analysis.

The frequency analysis algorithm we used is based on Laskar's original idea, named NAFF as Numerical Analysis of the Fundamental Frequencies (see for instance Laskar (1993) for the method, and Laskar (2005) for the convergence proofs). It aims at identifying the coefficients  $a_k$  and  $\omega_k$  of a complex signal  $f(t)$  obtained numerically over a finite time span  $[-T; T]$  and verifying

$$f(t) \approx \sum_{k=1}^n a_k \exp(i\omega_k t), \quad (28)$$

where  $\omega_k$  are real frequencies and  $a_k$  complex coefficients. If the signal  $f(t)$  is real, its frequency spectrum is symmetric and the complex amplitudes associated with the frequencies  $\omega_k$  and  $-\omega_k$  are complex conjugates. The frequencies and amplitudes associated are found with an iterative scheme. To determine the first frequency  $\omega_1$ , one searches for the maximum of the amplitude of

$$\phi(\omega) = \langle f(t), \exp(i\omega t) \rangle, \quad (29)$$

where the scalar product  $\langle f(t), g(t) \rangle$  is defined by

$$\langle f(t), g(t) \rangle = \frac{1}{2T} \int_{-T}^T f(t) \overline{g(t)} \chi(t) dt, \quad (30)$$

and where  $\chi(t)$  is a weight function, i.e. a positive function with

$$\frac{1}{2T} \int_{-T}^T \chi(t) dt = 1. \quad (31)$$

Once the first periodic term  $\exp(i\omega_1 t)$  is found, its complex amplitude  $a_1$  is obtained by orthogonal projection, and the process is started again on the remainder  $f_1(t) = f(t) - a_1 \exp(i\omega_1 t)$ . The algorithm stops when two detected frequencies are too close to each other, which alters their determinations, or when the number of detected terms reaches a maximum set by the user. This algorithm is very efficient, except when two frequencies are too close to each other. In that case, the algorithm is not confident in its accuracy and stops. When the difference between two frequencies is larger than twice the frequency associated with the length of the total time interval, the determination of each fundamental frequency is not perturbed by the other ones. Although the iterative method suggested by Champenois (1998) allows to reduce this distance, some difficulties remain when the frequencies are too close to each other.

### 3.4. Outputs

In order to deliver theories of rotation that can be easily compared with observations, we chose to express our results in the following variables:

- Longitudinal librations,
- Latitudinal librations,
- Orbital obliquity  $\epsilon$  (the orientation of the angular momentum of Mimas with respect to the normal to the instantaneous orbital plane),
- Motion of the rotation axis about the pole axis.

There are at least two ways to define the longitudinal librations. We can for instance consider the librations about the exact synchronous rotation, i.e.  $p - \langle n \rangle t$ , usually called physical librations. In this case, we have used for  $\langle n \rangle$  the frequency associated with the proper mode  $\lambda$ , i.e. Mimas' mean longitude. Another way to consider the longitudinal librations is to work on the librations about the Mimas-Saturn direction. We will call these librations tidal librations because they represent the misalignment of the tidal bulge of the satellite. The difference between these two librations is known as optical librations, only due to the orbital motion of Mimas around Saturn. The reader can find graphical descriptions of these librations in Murray & Dermott (1999), Fig.5.16.

The latitudinal librations are the North-South librations of the large axis of the considered body in the saturnocentric reference frame that follows the orbital motion of the body. They are analogous to the tidal librations that are the East-West librations. In order to get the tidal longitudinal librations and the latitudinal librations, we first should express the unit vector  $f_1$  (i.e. the direction of Mimas' long axis) in the inertial frame  $(e_1, e_2, e_3)$ . From (Eq.22) and the definitions of the Andoyer modified variables (Eq.15), we get:

$$\begin{aligned}
\mathbf{f}_1 = & (\cos r(\cos(p+r-l)\cos l - \sin(p+r-l)\cos J \sin l) \\
& + \sin r(\cos K(\sin(p+r-l)\cos l \\
& + \cos(p+r-l)\cos J \sin l) - \sin K \sin J \sin l)\mathbf{e}_1 \\
& + (-\sin r(\cos(p+r-l)\cos l - \sin(p+r-l)\cos J \sin l) \\
& + \cos r(\cos K(\sin(p+r-l)\cos l \\
& + \cos(p+r-l)\cos J \sin l) - \sin K \sin J \sin l)\mathbf{e}_2 \\
& + (\sin K(\sin(p+r-l)\cos l + \cos(p+r-l)\cos J \sin l) \\
& + \cos K \sin J \sin l)\mathbf{e}_3.
\end{aligned} \tag{32}$$

The tidal longitudinal librations  $\psi$  and the latitudinal ones  $\eta$  are found this way:

$$\psi = \mathbf{t} \cdot \mathbf{f}_1 \tag{33}$$

and

$$\eta = \mathbf{n} \cdot \mathbf{f}_1, \tag{34}$$

where  $\mathbf{n}$  is the unit vector normal to the orbit plane, and  $\mathbf{t}$  the tangent to the trajectory. We get these last two vectors by:

$$\mathbf{n} = \frac{\mathbf{x} \times \mathbf{v}}{\|\mathbf{x} \times \mathbf{v}\|} \tag{35}$$

and

$$\mathbf{t} = \frac{\mathbf{n} \times \mathbf{x}}{\|\mathbf{n} \times \mathbf{x}\|}, \tag{36}$$

where  $\mathbf{x}$  is the position vector of the body, and  $\mathbf{v}$  its velocity.

Finally, the motion of the rotation axis about the pole is derived from the wobble  $J$ , it is given by the two variables  $Q_1$  and  $Q_2$  defined as:

$$Q_1 = \sin J \sin l \left(1 + \frac{J_2 + 2C_{22}}{C}\right) \tag{37}$$

and

$$Q_2 = \sin J \cos l \left(1 + \frac{J_2 - 2C_{22}}{C}\right), \tag{38}$$

they are the first two components of the unit vector pointing at the instantaneous North Pole of Mimas' rotation axis, in the body frame of Mimas. These quantities are finally multiplied by the polar radius of the satellite, i.e. 190.6 km (Thomas, 2010) to get a deviation in meters.

## 4. Results

We here present the outputs of our numerical study of the rotation of Mimas. We first give the example of a non-hydrostatic model of Mimas based on its observed shape, then we compare the results with the rotational response of the first 22 models of Tab.2, obtained in considering Mimas to be in hydrostatic equilibrium.

### 4.1. Non-hydrostatic Mimas based on its shape

As already mentioned, this case is unique, because changes in the size of the core do not affect the ratios of the moments of inertia  $A/C$ , and  $B/C$ , and the coefficients  $\gamma_1$  and  $\gamma_2$  (Eq.17 and 18). As a consequence, there is a unique rotational behavior of

**Table 4.** Frequencies and periods of the free librations of Mimas, in the shape model. These values have been obtained numerically.

Proper mode	Frequency (rad/d)	Period $T$ (d)
$u$	2.704622	2.323129
$v$	0.778015	8.075914
$w$	0.621287	10.113182

Mimas for any homogenous or 2-layer model using this specific model based on the observed shape.

The free librations around the equilibrium are assumed to be damped, it is anyway important to know their frequencies  $\omega_u$ ,  $\omega_v$  and  $\omega_w$  (or periods  $T_u$ ,  $T_v$  and  $T_w$ ) because they characterize the way the system reacts to external sinusoidal excitations, that are here due to the variations of the distance between the Sun and Mimas.

The frequencies of the free librations are listed in Tab.4. The proper mode  $u$  roughly represents the free longitudinal librations,  $v$  the free librations of the obliquity, and  $w$  the wobble, i.e. the free polar motion of Mimas. These frequencies have been deduced from the frequency analysis of the modified Andoyer variables (cf.Eq.15).

So, the proper modes involved in the Fourier representations of the librations of Mimas are the forced modes due to the orbital motion of Mimas around Saturn (cf.Tab.3) and the free ones (Tab.4). The arguments of the sinusoidal components of the quasi-periodic decompositions of the variables of the rotation are integer combinations of these proper modes. If we consider that the free librations are damped, the solutions should be only composed of the forced modes.

The forced librations of Mimas modeled from its observed shape are given in Tab.5 to 8. These tables give the solutions under the form of periodic time series, in cosines. We can see that the main difference between the physical and the tidal librations is in the presence in the physical librations of a long-period term ( $\approx 70$  years) with a high amplitude ( $\approx 43^\circ$ , i.e.  $\approx 86^\circ$  peak-to-peak) due to the librations of the argument of the orbital resonance between Mimas and Tethys. As explained in Rambaux *et al.* (2010) and (2011), the amplitude of the long period librations are equal to the magnitude of the orbital perturbations because at long period the body is oriented toward the central planet. As a consequence, by analysing the tidal librations, the long period librations vanish. There is also a large difference in the amplitude given for the tidal and physical longitudinal librations. As explained above, this difference is due to optical librations, with amplitude  $2e \approx 3.8 \times 10^{-2}$  rad  $\approx 2.2^\circ$ .

The latitudinal librations of Mimas (Tab.7) are significantly smaller ( $\approx 2$  arcmin vs.  $2.5^\circ$  for the tidal longitudinal librations), and so could hardly be used in the framework of observations of the rotation of Mimas (except if there are free oscillations due to a recent unexpected excitation). The mean obliquity of Mimas (Tab.8) is of the same order of magnitude.

### 4.2. For a hydrostatic Mimas

We performed the same numerical study of the 22 hydrostatic configurations of Mimas given in Tab.2. The results are gathered in Tab.9. In this table, the amplitudes of the tidal and physical longitudinal librations indicated are related to the mode  $\lambda - \phi + \zeta$  (period: 0.944898 d), while the latitudinal ones are related to the mode  $\lambda + \phi - \zeta$  (period: 0.939962 d). The main physical reason

**Table 5.** Forced tidal longitudinal librations of Mimas, in the shape model. The series are in cosine.

$\lambda$	$\omega$	$\phi$	$\zeta$	Frequency (rad/y)	Period (d)	Amplitude (arcmin)	Phase at J2000
1	-	-1	1	2428.763080	0.944898	157.73363	-79.177°
1	1	-1	1	2428.852395	0.944863	5.72739	-116.201°
1	-1	-1	1	2428.673643	0.944933	4.05163	137.568°
2	-	-2	2	4857.526150	0.472449	1.83667	-68.313°
1	-	-	1	2438.960801	0.940947	1.32391	-148.065°

**Table 6.** Forced physical longitudinal librations of Mimas, in the shape model. The series are in cosine.

$\lambda$	$\omega$	$\phi$	$\zeta$	Frequency (rad/y)	Period (d)	Amplitude (arcmin)	Phase at J2000
-	1	-	-	0.08904538	25772.62777	43.61°	51.354°
-	3	-	-	0.26713614	8590.87592	43.261 arcmin	-25.913°
1	-	-1	1	2428.763080	0.944898	26.075 arcmin	101.355°
-	-	1	-	10.19765304	225.04526	7.828 arcmin	-157.744°
-	1	-1	-	10.10860766	227.02728	3.657 arcmin	-119.032°
-	1	1	-	10.28669842	223.09718	3.532 arcmin	-16.309°

**Table 7.** Forced latitudinal librations of Mimas, in the shape model. The series are in cosine.

$\lambda$	$\omega$	$\phi$	$\zeta$	Frequency (rad/y)	Period (d)	Amplitude (arcmin)	Phase at J2000
1	-	1	-1	2441.516177	0.939962	2.07096	77.130°
1	1	1	-1	2441.605507	0.939928	0.06829	39.984°
1	-1	1	-1	2441.426665	0.939997	0.0414	-66.603°

of these librations is the variations of the distance Mimas-Saturn during an orbital period.

In order to make the results more readable, we present them graphically in Fig.3. The plots present a clear dependency of the amplitudes of librations on the densities of the core and the shell. We can in particular notice that the longitudinal (i.e. tidal and physical) librations have a larger amplitude when the density of the core is lower, it is due to the fact that a concentration of the mass in the core lowers the moments of inertia of the body, and so tends to limit its amplitude of response to sollicitations. Finally we can see that the dependency on  $\rho_c$  is small for  $\rho_s = 1100\text{kg/m}^3$ , it is because in this case,  $\rho_s$  is close to the mean density of Mimas (i.e.  $1150.03\text{kg/m}^3$ ), as a consequence the core is small and Mimas is close to be homogeneous.

#### 4.3. A small polar motion

As for the other outputs, we present the forced polar motion of Mimas (i.e. after removal of the free wobble) as a sum of a trigonometric series (Tab.10). We can see that this motion is expected to be small, the highest amplitude being  $\approx 15$  meters. The sum of all these amplitudes can reach 40 meters, so we can consider these 40 meters as the upper bound of the polar motion. An analysis of the polar motions for the different hydrostatic Mimas do not exhibit significant differences.

## 5. Tidal Dissipation

This section is dedicated to study the influence of the tidal torque on the rotational motion of Mimas. We introduce the tidal torque in a Lagrangian formalism and follow the approach of Williams *et al.* (2001) and used recently in Rambaux *et al.* (2010) and Robutel *et al.* (2011). The starting equation is the angular mo-

mentum equation

$$\frac{d\mathbf{G}}{dt} + \boldsymbol{\omega} \wedge \mathbf{G} = \mathbf{T} \quad (39)$$

where  $\boldsymbol{\omega}$  is the angular velocity vector, the angular momentum  $\mathbf{G} = I\boldsymbol{\omega}$  with  $I$  the tensor of inertia, and  $\mathbf{T}$  is the external gravitational torque expressed as

$$\mathbf{T} = \frac{3GM_{\text{h}}}{r^3} \mathbf{u} \wedge I\mathbf{u} \quad (40)$$

where  $\mathbf{u}$  is the cosine director of Saturn in the reference frame tied to Mimas, and  $M_{\text{h}}$  its mass.

The dissipation is due to the tidal and centrifugal potentials that deform the satellite. In this case, the tensor of inertia  $I$  becomes a constant plus a time-variable part resulting from the deformation. The time-variable part does not react instantaneously and therefore presents a time delay  $\delta t$  characteristics of the rheological properties of the body (see section 2).

In addition, the dynamical equation of the rotational motion Eq. 39 may be linearized by using the synchronous spin-orbit resonance of the body implying that  $\omega_1, \omega_2 \ll \omega_3 \sim n$  and  $u_2, u_3 \ll u_1 \sim 1$  where  $u_1, u_2, u_3$  are the coordinates of the cosine director along the principal axis of inertia of Mimas.

By using these approximations and focusing on the libration in longitude, the main tidal torque is expressed as (Williams *et al.* 2001)

$$T_t = -k_2 R^5 \frac{3GM_{\text{h}}^2}{a^6} (U_{11}U_{12}^* - U_{12}U_{11}^*), \quad (41)$$

where  $U_{ij} = \left(\frac{a}{r}\right)^3 u_i u_j$  and the star indicates the time delay part.

Then, we used the same approach than in Rambaux *et al.* (2010). We introduce the rotation angle  $\varphi$  similar to the sum of the Andoyer angles  $l + g$  because the polar motion is small as

**Table 8.** Forced obliquity of Mimas, in the shape model. The series are in cosine.

$\lambda$	$\omega$	$\phi$	$\Phi$	Frequency (rad/y)	Period (d)	Amplitude (arcmin)	Phase at J2000
-	-	-	-	0	$\infty$	2.13468	-
2	-	1	-1	4883.032354	0.469981	0.07372	-27.144°
2	-1	1	-1	4882.943311	0.469990	0.07179	14.019°
2	1	1	-1	4883.121227	0.469973	0.06866	119.800°
-	2	-	-	0.177998	12893.06	0.04817	103.293°

**Table 9.** Periods of the free librations and amplitudes (in arcmin) of the forced librations for the different models assuming that Mimas is at the hydrostatic equilibrium.

N	$T_u$ (d)	$T_v$ (d)	$T_w$ (d)	Tidal librations (d)	Latitudinal librations	Mean obliquity	Physical librations
1	2.143878	7.885550	11.621674	163.398	2.016	2.086	31.744
2	2.294081	8.997072	13.222674	158.577	2.314	2.384	26.914
3	2.407777	9.908107	12.763086	155.609	2.559	2.631	23.944
4	2.468518	10.416095	13.618627	154.248	2.693	2.765	22.582
5	2.507237	10.742236	14.181571	153.442	2.780	2.853	21.776
6	2.534519	10.975456	14.591169	152.900	2.843	2.917	21.234
7	2.555063	11.152890	14.906138	152.508	2.891	2.966	20.841
8	2.138844	7.849766	11.569966	163.583	2.006	2.076	31.922
9	2.220696	8.443608	12.426948	160.777	2.166	2.234	29.115
10	2.257477	8.730512	12.839826	159.593	2.243	2.313	27.930
11	2.274983	8.851150	13.013162	159.124	2.275	2.346	27.461
12	2.284054	8.920304	13.112486	158.862	2.293	2.363	27.199
13	2.290031	8.966015	13.178106	158.692	2.306	2.378	27.028
14	2.294326	8.998974	13.225425	158.571	2.315	2.384	26.907
15	2.128297	7.775062	11.461869	163.975	1.986	2.054	32.314
16	2.154684	7.962727	11.733240	163.008	2.037	2.104	31.347
17	2.162067	8.015705	11.809777	162.745	2.051	2.119	31.084
18	2.164709	8.034707	11.837202	162.652	2.056	2.124	30.991
19	2.166135	8.044989	11.852091	162.602	2.059	2.127	30.941
20	2.167044	8.051527	11.861492	162.570	2.060	2.132	30.909
21	2.167685	8.056158	11.868221	162.548	2.062	2.130	30.886
22	2.106951	7.625231	11.244996	164.792	1.946	2.014	33.132

**Table 10.** Polar motion of Mimas  $q_1 + iq_2$ , in the shape model. The series are in complex exponentials.

$\lambda$	$\omega$	$\phi$	$\zeta$	$\Phi$	Frequency (rad/y)	Period (d)	Amplitude (m)	Phase at J2000
1	-	1	-1	-	2441.516177	0.939962	15.277	77.130°
-1	-	-1	1	-	-2441.516177	0.939962	14.368	102.870°
-	-	-1	-	1	-12.7530964	179.951077	4.498	113.654°
-	-	1	-	-1	12.7530964	179.951077	3.441	66.208°
1	1	1	-1	-	2441.605507	0.940313	0.503	40.052°
2	-	-1	2	-1	4870.2792464	0.471212	0.485	87.878°
-1	-1	-1	1	-	-2441.605507	0.940313	0.473	139.948°

shown in Figure 2 where  $J$  and  $\theta$  (the nutation angle) are small. The libration angle  $\gamma$  is defined as  $\varphi = M + \gamma$  representing the physical libration in longitude of the body. The cosine director  $u_2 \sim s - \gamma$  is of the order of the difference between the orbital variation  $s$  and the physical libration  $\gamma$ . We note that  $u_2$  corresponds to the tidal libration  $\psi$  defined in section 3.4 and their amplitude is small as shown in Table 5. The quantity  $s$ , the orbital variation, is defined as the difference between the true and the mean longitude of Mimas and represents the oscillation of the orbital longitude of Mimas that may be expressed in Fourier series as

$$s = \sum_i H_i \sin(\omega_i t + \alpha_i). \quad (42)$$

Then, by developing  $u_1^*$  and  $u_2^*$  in Taylor series for small  $\delta t$ , the dynamical equation becomes:

$$C\ddot{\gamma} + \frac{3}{2}(B-A)\frac{Gm}{r^3} \sin 2(\gamma - s) = -k_2 R^5 \frac{3GM^2}{a^6} \delta t (\dot{\gamma} - \dot{s}). \quad (43)$$

As shown in the previous section, the quantity  $\gamma - s$  is always small (see Table 5) allowing to simplify the sine function by its angle. In addition, the eccentricity of Mimas is small and so  $a/r$  is equal to 1 at first order in eccentricity. Finally, we obtain a forced dissipative harmonic oscillator with the frequency  $\omega_0 = n\sqrt{3(B-A)/C}$  and the dissipative rate  $\lambda$  expressed as

$$2\lambda = \frac{3k_2 R^3}{C} \frac{n^4}{Gm} \delta t, \quad (44)$$

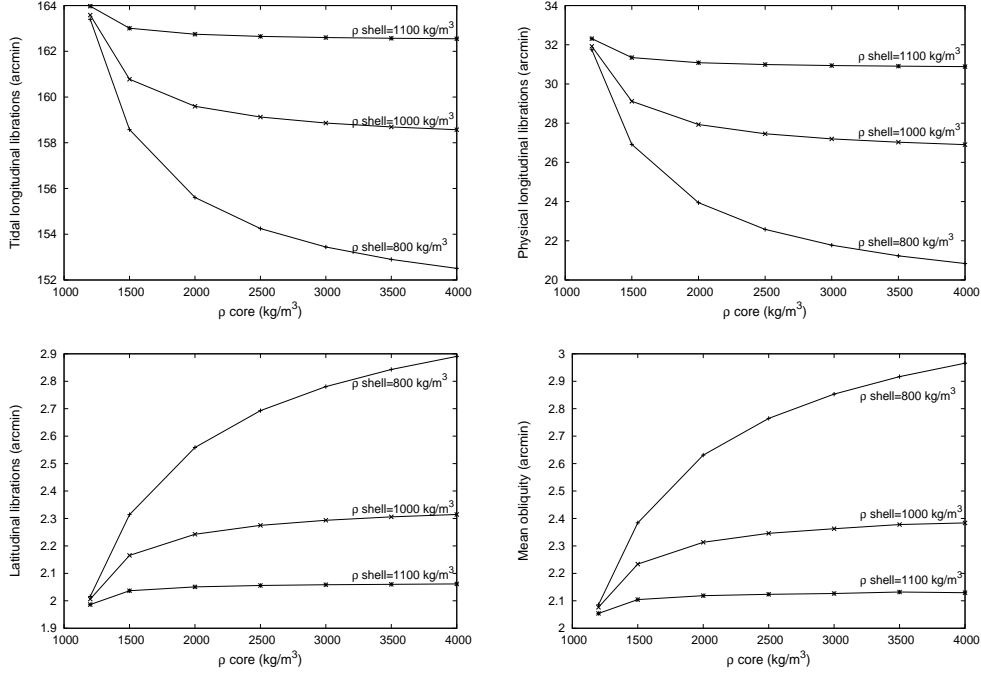


**Fig. 3.** Librations of hydrostatic Mimas, depending on the densities of the core and the shell.

$m$  being the mass of the satellite and  $k_2$  is the Love number of Mimas.

As for the conservative case, the amplitude of terms associated with the long period is almost equal to the magnitude of the oscillation  $s$ . The solution may be expressed as

$$\gamma = A_d \sin(\omega_d t + \phi_d) e^{-\lambda t} + \sum_i x_i \cos(\omega_i t + \alpha_i) + y_i \sin(\omega_i t + \alpha_i), \quad (45)$$

where  $A_d$  and  $\phi_d$  are constants of integration. The first term decays with time scale  $1/\lambda$  and its resonant frequency is  $\omega_d = \sqrt{\omega_0^2 - \lambda^2}$ . The periodic term of the particular solution  $\gamma$  is composed of the in-phase  $y_i$  and out-of-phase  $x_i$  terms

$$y_i = H_i \frac{(\omega_0^2 - \omega_i^2)\omega_0^2 + 4\lambda^2\omega_i^2}{(\omega_0^2 - \omega_i^2)^2 + 4\lambda^2\omega_i^2}, \quad x_i = H_i \frac{-2\lambda\omega_i^3}{(\omega_0^2 - \omega_i^2)^2 + 4\lambda^2\omega_i^2}. \quad (46)$$

At first order, the expression of  $x_i$  may be simplified as

$$x_i = -0.9054 \frac{k_2}{Q} H_i \frac{\omega_i^3}{(\omega_0^2 - \omega_i^2)^2} \quad (47)$$

expressed in radians and by introducing the dissipation factor as  $\delta t = (nQ)^{-1}$ . For short period librations at 0.944898 days the  $x_i$  is 1.32 mas with  $\frac{k_2}{Q} = 10^{-6}$  (this is the value used by Meyer & Wisdom (2008)) and the resulting displacement at the surface of the satellite at the periaster passage is also negligible 0.0013 m. The damping time  $1/\lambda$  is about 6,000 years. If we consider  $\frac{k_2}{Q}$  to be 100 times bigger, i.e. closer to the expected value of Enceladus, we have a displacement at the surface of  $\approx 0.13$  m and a damping time of  $\approx 60$  years. For librations at long period  $x_i$  is definitely negligible because  $\omega_i$  is very small.

## 6. Discussion

One of the aims of this theoretical study is to prepare the interpretation of potential observations of the rotation of Mimas.

After a restricted analytical approach to validate the numerical results, we discuss the possibility to observe the rotation of Mimas and in particular to discriminate the different interior models. Then we focus on the non-hydrostatic contributions.

### 6.1. Analytical approach

We here compare with classical analytical formulae for the main term of the physical and tidal longitudinal librations and the mean obliquity, for which deriving accurately these amplitudes is quite straightforward.

#### 6.1.1. Longitudinal librations

An analytical study of the longitudinal librations of a satellite in 1:1 spin-orbit resonance and on a keplerian orbit can be found for instance in Murray & Dermott (1999). Let us call  $\psi$  the amplitude of the main term (i.e. associated with the mode  $\lambda + \phi - \zeta$ ) of the tidal librations, and  $\gamma$  for the physical ones. We have from Murray & Dermott (1999):

$$\psi = \frac{-2e}{1 - \left(\frac{\omega_u}{n}\right)^2}, \quad (48)$$

$$\gamma = \frac{2e}{1 - \left(\frac{n}{\omega_u}\right)^2}, \quad (49)$$

$$(50)$$

and

$$\left(\frac{\omega_u}{n}\right)^2 = 3 \frac{B-A}{C} \left(1 - 5e^2 + \frac{13}{16}e^4\right) = 12 \frac{C_{22}}{C/(mR^2)} \left(1 - 5e^2 + \frac{13}{16}e^4\right), \quad (51)$$

$e$  being the eccentricity of Mimas. We can see that this amplitude is bigger when the ratio is closer to unity, or when  $12C_{22}$  is closer

to  $C/(mR^2)$ . We can see from the Tab.2 that  $C_{22}$  is of the order  $5 \times 10^{-3}$  while  $C \approx 0.4mR^2$ , i.e.  $C_{22}/C/(mR^2) \approx 1/80$ . Thus, the ratio  $12 \frac{C_{22}}{C/(mR^2)}$  is closer to unity when  $C_{22}$  is bigger, what is the case for the smallest values of  $\rho_c$ . The Fig.3 confirms this trend, while the Tab.11 settles the validity of the analytical formulae (48) and (49).

### 6.1.2. Mean obliquity

We here use the analytical study of Ward & Hamilton (2004) (see Noyelles (2010) for an application to natural satellites in spin-orbit resonances) for the location of the Cassini States. Mimas is expected to be locked at the Cassini State 1, i.e. the most stable one, characterized by:

$$\epsilon = -\frac{\sin I}{\frac{3n}{2\delta\dot{\Omega}} \frac{J_2+2C_{22}}{C/(mR^2)} + \cos I}, \quad (52)$$

$\epsilon$  being the mean obliquity of Mimas,  $\delta\dot{\Omega}$  the precessional rate of its orbital ascending node, and  $I$  its inclination on the Laplace Plane, here assumed to be the equator of Saturn at J2000.

From the definition the orbital proper modes of Mimas, we can approximate  $\delta\dot{\Omega}$  by  $\dot{\Phi} - \dot{\zeta} = -6.37188169$  rad/y, this yields a regressional period of 360.1657 days. In assuming  $J_2 \approx 2 \times 10^{-2}$ ,  $C_{22} \approx 6 \times 10^{-3}$  and  $C \approx 0.4mR^2$  from Tab.2, we have  $\frac{3n}{2\delta\dot{\Omega}} \frac{J_2+2C_{22}}{C/(mR^2)} \approx -37.26$  while  $\sin I$  is very small and  $\cos I$  close to unity (the mean inclination of Mimas  $I$  being of the order of  $1.5^\circ = 2.6 \times 10^{-2}$  rad). So, bigger values of the quantity  $J_2 + 2C_{22}$  will yield a smaller obliquity. Once more, these values are reached for the lowest estimations of  $\rho_c$ , the Fig.3 confirming this tendency. The validity of the analytical formula (52) is checked in Tab.11.

The analytical validation meets the following trouble: how to evaluate the mean eccentricity and inclination required in the analytical formulae, i.e. how to average them? These formulae have been derived in assuming a Keplerian orbit, while the orbit of Mimas is perturbed by the oblateness of Saturn and the mutual interactions with the other satellites, inducing an orbital resonance with Tethys. As a consequence, its eccentricity and inclination are far from constant.

We have, from Vienne & Duriez (1995):

$$\begin{aligned} z(t) &= e(t) \exp(i\varpi(t)) \\ &= 1.59817 \times 10^{-2} \exp(i(6.38121472t + 356.521^\circ)) \\ &+ 7.2147 \times 10^{-3} \exp(i(6.29216934t + 137.197^\circ)) \quad (53) \\ &+ 7.1114 \times 10^{-3} \exp(i(6.47026010t + 35.846^\circ)) + \dots, \end{aligned}$$

$$\begin{aligned} \zeta(t) &= \sin\left(\frac{I(t)}{2}\right) i\delta\dot{\Omega}(t) \\ &= 1.18896 \times 10^{-2} \exp(i(-6.37188169t + 234.213^\circ)) \\ &+ 5.3177 \times 10^{-3} \exp(i(-6.46092707t + 14.888^\circ)) \quad (54) \\ &+ 5.3017 \times 10^{-3} \exp(i(-6.28283631t + 273.538^\circ)) + \dots, \end{aligned}$$

the frequencies being in rad/year, and the time origin J1980. As we can see, the mean eccentricity should be at least  $\approx 1.6 \times 10^{-2}$ , probably higher (same for the mean inclination, that should be at least  $\approx 1.4^\circ$ ). In the Tab.11, we use  $e = 1.92 \times 10^{-2}$  and  $I = 1.68^\circ$ , this arbitrary choice minimizes the relative errors and is consistent with the TASS1.6 theory.

### 6.2. Observational possibilities

It would be challenging to constrain the orientation and interior structure of Mimas using its rotation. The first expected result is the confirmation that Mimas is in the Cassini State 1 with the 1:1 spin-orbit resonance. Another challenge would be to detect the longitudinal librations, that have been actually observed for the Moon (Koziel (1967)), the Martian satellite Phobos (Burns (1972)), and the Saturnian satellite Epimetheus (Tiscareno et al. (2009)). To estimate the required accuracy of the observations, we convert the rotation outputs into kilometres (Tab.12).

**Table 12.** Expected librations and mean obliquity of Mimas, in km. The mean obliquity  $\epsilon$  has been multiplied by the polar radius  $c = 190.6$  km, while the librations have been multiplied by the Saturn-facing radius  $a = 207.8$  km. The case 23 is derived from the shape model.

N	Physical librations	Tidal librations	Latitudinal librations	Mean Obliquity
1	1.919	9.877	0.122	0.116
2	1.627	9.585	0.140	0.132
3	1.447	9.406	0.155	0.146
4	1.365	9.324	0.163	0.153
5	1.316	9.275	0.168	0.158
6	1.284	9.242	0.172	0.162
7	1.260	9.219	0.175	0.164
8	1.930	9.888	0.121	0.115
9	1.760	9.718	0.131	0.124
10	1.688	9.647	0.136	0.128
11	1.660	9.618	0.138	0.130
12	1.644	9.603	0.139	0.131
13	1.634	9.592	0.139	0.132
14	1.626	9.585	0.140	0.132
15	1.953	9.912	0.120	0.114
16	1.895	9.853	0.123	0.117
17	1.879	9.837	0.124	0.117
18	1.873	9.832	0.124	0.118
19	1.870	9.829	0.124	0.118
20	1.868	9.827	0.125	0.118
21	1.867	9.825	0.125	0.118
22	2.003	9.961	0.118	0.112
23	1.576	9.534	0.125	0.118

As expected, the longitudinal librations are significantly bigger (a few kilometres) than the mean obliquity and the latitudinal librations (with an amplitude smaller than 200 meters). The amplitude of the librations given are related to the quasi-periodic decompositions, so the peak-to-peak amplitudes are twice bigger. The reader should keep in mind that the physical and tidal librations are two expressions of the same quantity, so are not independent. We can consider that the detection of the longitudinal librations would require an accuracy of about 1 km, while using them to invert the internal structure of Mimas would require an accuracy at least ten times better.

### 6.3. Non-hydrostatic contributions

The study of the non-hydrostatic Mimas, based on the shape model, does not exhibit a significant possibility to discriminate a non-hydrostatic Mimas from a hydrostatic one from observations. This is not surprising considering Mimas' nearly hydrostatic global shape. But a non-hydrostatic Mimas could result in an offset between the ellipsoid of shape and the ellipsoid of inertia, as investigated for Janus by Robutel et al. (2011), for which

**Table 11.** Analytical confirmation of the numerical results given in Tab.2. The analytical formulae used are Eq.51, 49, 48 & 52, the obtained values being compared with the ones given in Tab.9.

N	$T_u$ (d)	$\Delta T_u$	$\gamma$ (arcmin)	$\Delta\gamma$	$\psi$ (arcmin)	$\Delta\psi$	$\epsilon$ (arcmin)	$\Delta\epsilon$
1	2.145171	0.060%	31.572	0.542%	163.581	0.112%	2.088	0.104%
2	2.294910	0.036%	26.778	0.506%	158.787	0.133%	2.397	0.547%
3	2.410238	0.102%	23.825	0.497%	155.835	0.145%	2.651	0.741%
4	2.471008	0.101%	22.471	0.493%	154.480	0.150%	2.790	0.890%
5	2.509751	0.100%	21.669	0.490%	153.679	0.154%	2.880	0.956%
6	2.537080	0.101%	21.131	0.487%	153.140	0.157%	2.945	0.966%
7	2.557614	0.100%	20.740	0.487%	152.749	0.158%	2.994	0.960%
8	2.140163	0.062%	31.755	0.522%	163.765	0.111%	2.078	0.108%
9	2.221696	0.045%	28.965	0.514%	160.975	0.123%	2.243	0.411%
10	2.259963	0.110%	27.788	0.508%	159.798	0.128%	2.323	0.429%
11	2.275851	0.038%	27.321	0.508%	159.331	0.130%	2.356	0.446%
12	2.284904	0.037%	27.061	0.507%	159.071	0.131%	2.376	0.537%
13	2.290872	0.037%	26.892	0.505%	158.901	0.132%	2.388	0.438%
14	2.295156	0.036%	26.771	0.506%	158.780	0.132%	2.398	0.569%
15	2.129674	0.065%	32.145	0.522%	164.155	0.110%	2.057	0.170%
16	2.155925	0.058%	31.184	0.522%	163.193	0.113%	2.110	0.266%
17	2.163275	0.056%	30.922	0.520%	162.932	0.115%	2.124	0.251%
18	2.165905	0.055%	30.830	0.520%	162.839	0.115%	2.130	0.263%
19	2.167325	0.055%	30.780	0.520%	162.789	0.115%	2.132	0.256%
20	2.168230	0.055%	30.748	0.520%	162.758	0.116%	2.134	0.106%
21	2.168868	0.055%	30.726	0.518%	162.736	0.115%	2.136	0.261%
22	2.108464	0.074%	32.958	0.526%	164.967	0.106%	2.016	0.095%

an offset in longitude and in latitude has actually been detected (Tiscareno et al. (2009)). So, detection of non-hydrostatic contributions from observation of Mimas' orientation should not a priori be excluded.

## 7. Conclusion

We have presented a theoretical study of the rotation of Mimas, in considering the 3 degrees of freedom of the rigid rotation, and different possible interior models, in assuming Mimas to be in hydrostatic equilibrium, or not. Moreover, we have considered a complete orbital motion, and also investigated the influence of tides on the rotation of Mimas.

We estimate the physical longitudinal librations to have an amplitude of about  $0.5^\circ$ , i.e. nearly 2 km, the exact value depending on the internal structure of Mimas. For a hydrostatic Mimas, a dense core lowers this amplitude. Non-hydrostatic contributions are shown to be small as expected from Mimas shape in near hydrostatic equilibrium. Moreover, we expect an obliquity between 2 and 3 arcmin, while the polar motion can be neglected. The tidal deviation of Mimas' long axis should be negligible as well, while this is the most inner main Saturnian satellite.

The Cassini spacecraft has already completed its initial four-year mission and the first extended mission, with a limited number of Mimas flybys. Its orbit close to Saturn makes Mimas a difficult target for Cassini observations. Since September 2010 Cassini is in a second extended mission called the Cassini Solstice Mission during (and especially at the end) of which Cassini will likely have additional Mimas observations. We hope that future observations of Mimas will allow us to constrain its rotation and to get clues on its internal structure and orientation.

## Appendix A: Notations used in the paper

**Acknowledgements.** Numerical simulations were made on the local computing resources (Cluster URBM-SYSDYN) at the University of Namur. This work has been supported by EMERGENCE-UPMC grant (contract number: EME0911).

## References

- Allan R.R., 1969, *AJ*, 74, 497  
 Andoyer H., 1926, *Mécanique céleste*, Gauthier-Villars, Paris, in French  
 Arnold V.I., 1963, *Uspekhi Mat. Nauk.*, 18, 13, in Russian. English translation: *Russian Mathematical Surveys*, 18, 9  
 Burns J.A., 1972, *Rev. Geophys. Space Phys.*, 10, 463  
 Cassini G.D., 1693, *Traité de l'origine et du progrès de l'astronomie*, Paris, in French  
 Champenois S., 1998, *Dynamique de la résonance entre Mimas et Thétyhs, premier et troisième satellites de Saturne*, Ph.D Thesis, Observatoire de Paris, in French  
 Champenois S. & Vienne A., 1999a, *Icarus*, 140, 106  
 Champenois S. & Vienne A., 1999b, *Cel. Mech. Dyn. Astr.*, 74, 111  
 Colombo G., 1966, *AJ*, 71, 891  
 Comstock R.L. & Bills B.G., 2003, *J. Geophys. Res.*, 108(E09), 5100  
 Deprit A., 1967, *American Journal of Physics*, 35, 424  
 Dermott S.F. & Thomas P.C., 1988, *Icarus*, 73, 25  
 Eluszkiewicz J., 1990, *Icarus*, 84, 215  
 Henrard J., 2005a, *Icarus*, 178, 144  
 Henrard J., 2005b, *Cel. Mech. Dyn. Astr.*, 91, 131  
 Henrard J., 2005c, *Cel. Mech. Dyn. Astr.*, 93, 101  
 Howett C.J.A., Spencer J.R., Schenk P., Johnson R.E., Paranicas C., Hurford T., Verbiscer A. & Segura M., 2011, *Icarus*, in press, doi:10.1016/j.icarus.2011.09.007  
 Hubbard W.B. & Anderson J.D., 1978, *Icarus*, 33, 336  
 Jacobson R.A., Antreasian P.G., Bordi J.J., Criddle K.E., Ionasescu R., Jones J.B., Mackenzie R.A., Pelletier F.J., Owen Jr. W.M., Roth D.C. & Stauch J.R., 2006, *AJ*, 132, 2520  
 Johnson T.V., Castillo-Rogez J. & Matson D.L., 2006, *DPS meeting 38*, 69.03, *BAAS*, 38, 621  
 Koziel K., 1967, *Icarus*, 7, 1  
 Lambeck K. & Pullan S., 1980, *Phys. Earth Planet. Interiors*, 22, 29  
 Laskar J., 1993, *Cel. Mech. Dyn. Astr.*, 56, 191-196  
 Laskar J., 2005, *Frequency map analysis and quasiperiodic decomposition*, in *Hamiltonian systems and fourier analysis: new prospects for gravitational dynamics*, Benest et al. editors, Cambridge Sci. Publ., 99  
 Meyer J. & Wisdom J., 2008, *Icarus*, 193, 213

**Table A.1.** Notations used in the paper.

Physical parameters	
$R, R_c$	Mean radius of Mimas and of its core
$m$	Mass of Mimas
$a > b > c$	Radii of Mimas
$A < B < C$	Moments of inertia of Mimas
$A_c < B_c < C_c$	Moments of inertia of the core of Mimas
$\rho_c > \rho_s$	Densities of the core and the shell of Mimas
$k_f$	Fluid Love number of Mimas
$k_2$	Love number of Mimas
$J_2 = -C_{20}, C_{22}$	Gravity coefficients of Mimas
Proper modes	
$\lambda, \omega, \phi, \zeta, \Phi$	Orbital modes
$n$	Orbital and spin frequency of Mimas
$u, v, w$	Rotational modes, respectively in longitude, latitude and wobble
$\omega_u, \omega_v, \omega_w$	Frequencies of the rotational modes
Rotation variables	
$l, g, h, L, G, H$	Andoyer variables and the moments associated
$p, r, \xi_q, P, \mathcal{R}, \eta_q$	Modified Andoyer variables and the moments associated
Rotation outputs	
$\Psi$	Tidal longitudinal librations
$\gamma$	Physical longitudinal librations
$\eta$	Latitudinal librations
$\epsilon$	Obliquity of Mimas
$Q_1 + iQ_2$	Polar motion of Mimas
Tidal data	
$\lambda$	Dissipative rate
$x_i, y_i$	Displacement of the equilibrium

- Moser J., 1962, *Nachr. Akad. Wiss. Göttingen, Math. Phys.*, 2, 1
- Munk W.H. & MacDonald G.J., 1960, *The rotation of the Earth: A geophysical discussion*, Cambridge University Press, Cambridge
- Murray C.D. & Dermott S.F., 1999, *Solar System Dynamics*, Cambridge University Press, Cambridge
- Nekhoroshev N.N., 1977, *Russian Mathematical Surveys*, 32, 1
- Nekhoroshev N.N., 1979, *Trudy Sem., Petrov.*, 5, 5
- Noyelles B., Lemaître A. & Vienne A., 2008, *A&A*, 478, 959
- Noyelles B., 2010, *Icarus*, 207, 887
- Noyelles B., Delsate N. & Carletti T., 2011, *Equilibrium search algorithm of a perturbed quasi-integrable system: NAFFO*, submitted, arXiv:1101.2138
- Rambaux N., Castillo-Rogez J.C., Williams J.G. & Karatekin Ö., 2010, *Geophys. Res. Lett.*, 37, L04202
- Rambaux N., Van Hoolst T. & Karatekin Ö., 2011, *A&A*, A118
- Rappaport N., Bertotti B., Giamperi G. & Anderson J.D., 1997, *Icarus*, 126, 313
- Roatsch Th., Wählisch M., Hoffmeister A., Kersten E., Matz K.-D., Scholten F., Wagner R., Denk T., Neukum G., Helfenstein P. & Porco C., 2009, *Planet. Space Sci.*, 57, 83
- Robutel, P., Rambaux N., & Castillo-Rogez J.C., 2011, *Icarus*, 211, 758-769
- Struve H., 1891, *MNRAS*, 51, 251
- Thomas P.C., Burns J.A., Helfenstein P., Squyres S., Veverka J., Porco C., Turtle E.P., McEwen A., Denk T., Giese B., Roatsch T., Johnson T.V. & Jacobson R.A., 2007, *Icarus*, 190, 573
- Thomas P.C., 2010, *Icarus*, 208, 395
- Tiscareno M.S., Thomas P.C. & Burns J.A., 2009, *Icarus*, 204, 254
- Vienne A. & Duriez L., 1995, *A&A*, 297, 588
- Ward W.R. & Hamilton D.P., 2004, *AJ*, 128, 2501
- Yasui M. & Arakawa M., 2009, *J. Geophys. Res.*, 114, E09004
- Zebker H.A., Stiles B., Hensley S., Lorenz R., Kirk R.L. & Lunine J., 2009, *Science*, 324, 921-923

